Studies of the Scintillating Tileboards for the HGCAL-CMS Upgrade

Marie Christin Muehlnikel, University of Heidelberg

September 16, 2021

Abstract

As a part of the HL-LHC Phase II Upgrade, the endcaps of the CMS detector at CERN will be replaced with a new highly granular calorimeter (HGCAL). The hadronic calorimeter of the HGCAL will be based on silicon detectors and scintillator tileboards. These tileboards consists of scintillating tiles placed on top of SiPMs. As the working temperature in CMS will be at -30 °C, the main motivation for the temperature studies conducted was to ensure that the tileboard works stable at such low temperatures. A description of the used setup as well as the analyses methods and measurement results can be found in this report. The $(\frac{\Delta OV}{\Delta T})$-gradient was measured to be approximately $(33 \pm 2) mV/K$ for $2\,\mathrm{mm}^2$ non-irradiated SiPMs and $(31 \pm 1) mV/K$ for $4\,\mathrm{mm}^2$ non-irradiated SiPMs. For the irradiated SiPMs, the temperature dependence of the noise level was investigated.

Contents

1 Introduction

The CMS (Compact Muon Solenoid) is a general-purpose detector at the LHC. It has a broad research program, e.g. studying the Standard Model, the Higgs boson as well as the search for extra dimensions and dark matter. [1] At the moment, preparations for the HL-LHC Phase II Upgrade, which will integrate ten times more luminosity than the LHC, are ongoing. As part of this upgrade, the CMS endcaps will be replaced. The new HGCAL (High Granularity Calorimeter) aims for an improved energy and spatial resolution to overcome expected pile-up. As demonstrated in figure 1, the calorimeter consists out of two major components, the electromagnetic (CE-E) and hadronic calorimeter (CE-H). Whereas the electromagnetic calorimeter is based on silicon detectors, the latter one consists of silicon detectors and scintillator tileboards.

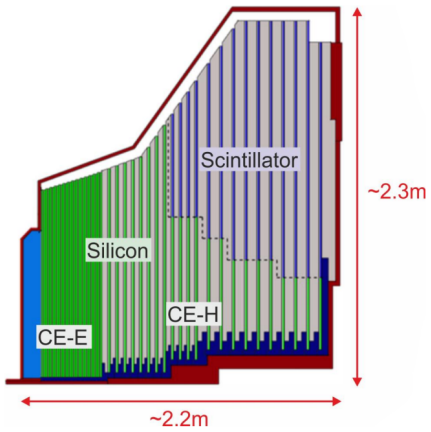

Figure 1: Cross section of the CMS-HGCAL endcap[2]

The new endcap of the hadronic calorimeter consists of 21 layers of tileboards in different trapezodial geometries. Each tileboard consists of 64 channels, which themselves consist of Scintillating Tiles glued on Silicon Photomultipliers (SiPMs). (See figure 2)

A single SiPM consists of a matrix of Single Photon Avalanche Diodes (SPAD), as sketched in figure 3. A SPAD is a semiconductor device based on two pn-junctions: one for absorption and one for multiplication. A photon passing the absorption zone creates an electron-hole pair, the electron then drifts further towards the multiplication region. Due to the high electric field in this area, the electrons are accelerated and - because of ionization - secondary electrons emerge, which themselves are accelerated and so on. This leads to an electron avalanche, which results in a discharge of the SPAD creating an observable signal. The voltage above which an avalanche can occur is known as breakdown voltage. The difference between the supplied voltage (bias voltage) and the breakdown voltage is known as overvoltage (OV): $OV = V_{bias} - V_{breakdown}$.

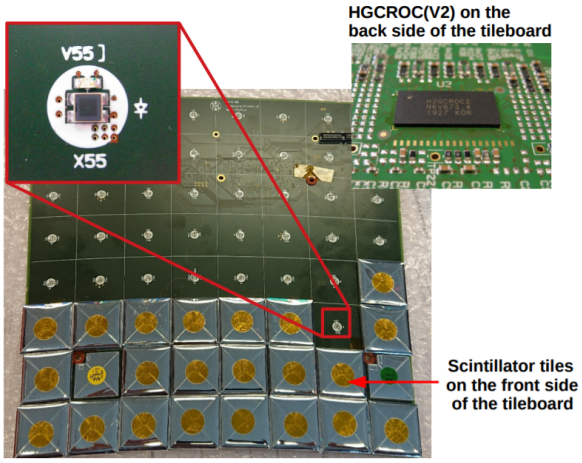

Figure 2: Tileboard[3]

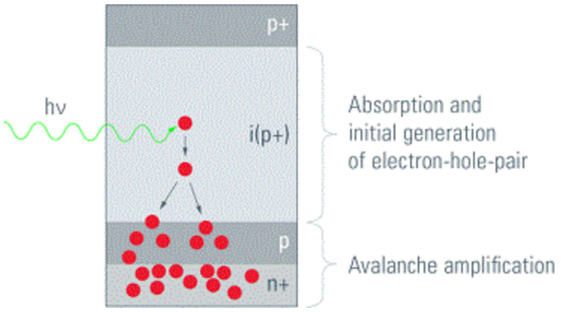

Figure 3: Conceptional structure of a SPAD[4]

A wrapped scintillating tile is glued on top of a SiPM and together these two components form a SiPM-on-tile. If charged particles pass the Scintillator Tile, photons are released and transferred to an electric signal by the SiPM (figure 4). Finally, the signals are readout using the onboard readout chip (HGCROC).

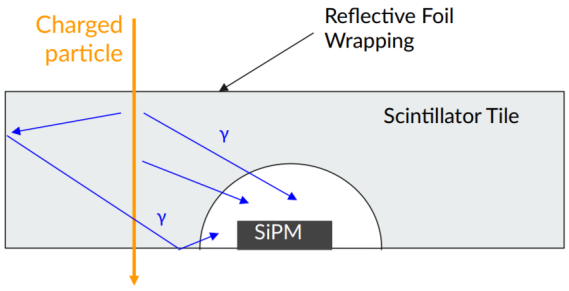

Figure 4: Cross-section of a tile-channel[3]

Each photon can create a discharge in a single SPAD in the SiPM. If multiple such SPADs undergo a discharge, the signal will correspond to the sum of all charge discharged by the SPADs resulting in a larger signal. By using a low intensity LED placed next to the SiPM, it is possible to create avalanches in a very few SPADs. If enough data is collected and the charge collected is plotted in a histogram, this will take the shape of a Single Photon Spectrum (SPS) as shown in figure 5, with each Gaussean peak corresponding to the number of photos excited per LED event. An important measurand is the mean distance between the peaks, the so called gain.

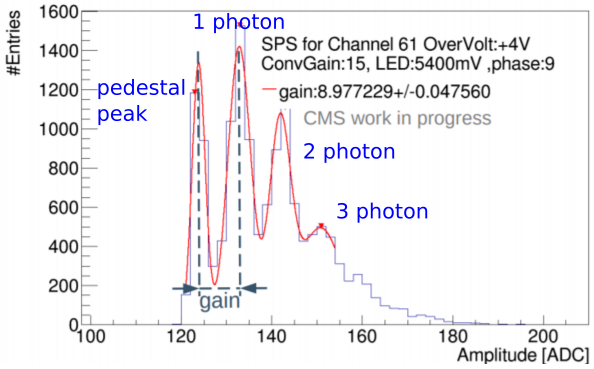

Figure 5: Example of an SPS[3]

Most of the further studies are based on the measurement of the SPS and the extraction of the gain. As the working temperature in CMS will be at -30 °C, the main motivation for the temperature studies conducted was to ensure that the tileboard works stable at such low temperatures.

2 Setup

As seen from figures 6 and 7, the tileboard was placed inside a climate chamber and was connected to the DAQ (data acquisition system) outside the chamber through a cable feedthrough. The DAQ delivers binary files with voltage and time information. Additionally, a voltage adapter is used in order to keep the SiPM voltage constant.

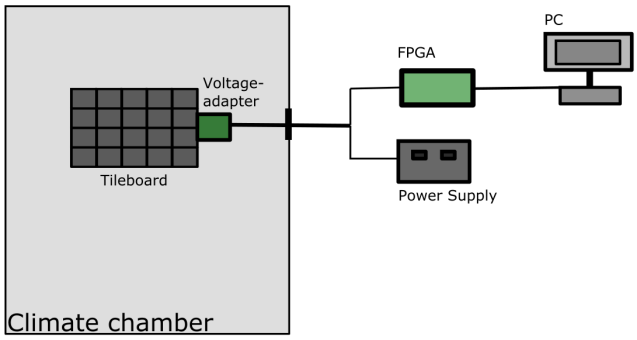

Figure 6: General concept of the temperature setup

Figure 7: Climate chamber

In order to make the setup light-tight, black cloths were used in- and outside the climate chamber, as shown in figures 8 and 9.

Figure 8: Light protection covering chamber

Figure 9: Light protection covering tileboard

Another crucial point that had to be taken care of was the humidity. When first cooled down to -30 $°C$, air got sucked in the chamber through the cable feedthrough, which led to visible ice inside the chamber (figure 10). Furthermore, while heating up to room temperature, there were visible water droplets on the glass pane . To resolve this issues, the chamber was flooded with dry air from an external supply to avoid condensation and additional tape was applied to the cable feedthrough to make it air-tight.

Figure 10: Ice inside the chamber

Once all the corrections were added, the setup was cooled down to -40$°C$ and the tileboard was rechecked if it worked in a stable way.

3 Temperature studies of non-irradiated SiPMs

For the first set of measurements - the temperature studies of non-irradiated SiPMs - a tileboard with 16 equipped channels was used. Half of those channels consists of 2 mm^2 SiPMs, the other half out of 4 mm^2 SiPMs.

3.1 Analysis

Before describing in more detail the different measurements that were applied, a description of the analysis work shall be given. The binary files received from the HGCROC via the DAQ system were converted into a ROOT tree and a fit of the SPS-spectra was applied on the data using ROOT's TSpectrum class. The results were converted to a Python pandas dataframe which was used for the main analysis.

Another issue that had to be faced is the Differential Non-Linearity (DNL) of the HGCROC. DNL is an electrical characteristic of an ADC (Analog-to-Digital-Converter). In the ideal case, an increase of the analog signal by one 'analog unit' should result in an increase of the output by one unit as well. However, due to technical limitations, ADCs are not ideal. Therefore, one step in 'analog units' is not always 'translated' into one step in 'digital units'. Additionally, the size of this 'translation error' can vary from step to step.

For the first time, a method to correct for the Differential Non-Linearity was applied successfully on the measured data. For the measurements described here, the DNL effects the data in a way that every odd ADC tick varies in size, which leads to the effect that every second bin receives systematically more entries. An SPS example before applying the DNL-correction can be seen in figure 11. As one can see, the single peaks do not have a proper gaussian form. A corrected version was achieved by taking data at different pedestal values (figure 12). Shifting and adding those spectra provides reasonable Gaussian peaks as seen in figure 13.

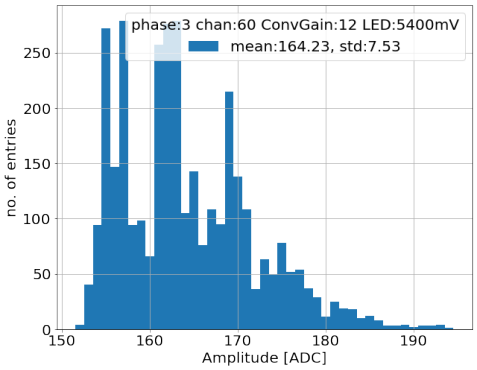

Figure 11: SPS before DNL correction

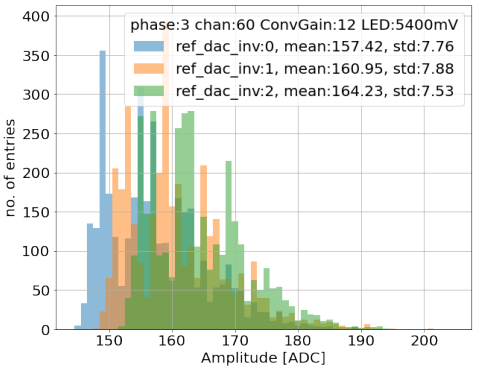

Figure 12: SPS at different reference values

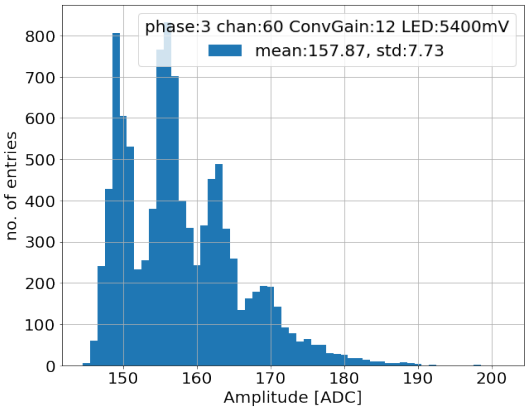

Figure 13: SPS after DNL correction

During the analysis process, additional issues concerning the fit and applied cuttings occurred. As described earlier, a fit of the SPS-spectra was applied, that was originally developed for data with much higher gain. As the gain of the here measured data was too low for a stable fitting, a large fraction of fits did not converge. Additionally, the χ^2- cuts exposed as not suitable in many cases, as two different effects occurred. First, a comparable low χ^2-value was possible, even though the spectrum was not resolved (figure 14). Second, a high χ^2- value was possible, even though the spectrum was well resolved (figure 15). The latter case especially occurred when peaks were found by the code, but could not be fitted properly. To circumvent this issues, the data had to be cut manually. Later on, the high χ^2-issue could be reduced significantly by code optimization, so that the evaluation now works for large data samples without the need of time-consuming manual cuttings.

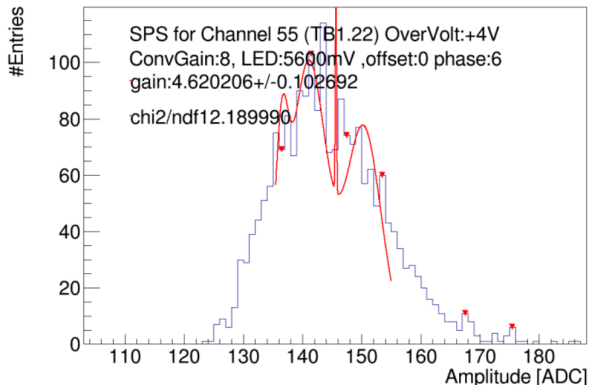

Figure 14: Bad fit example (1)

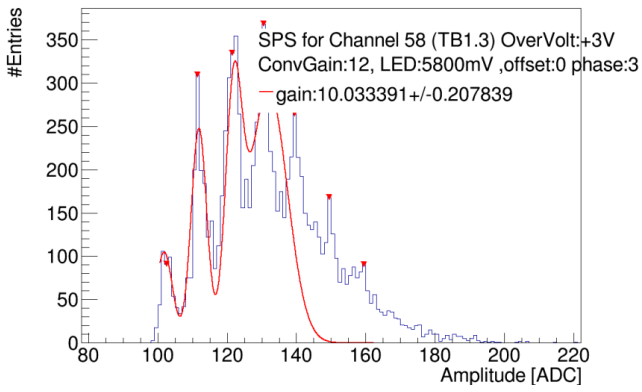

Figure 15: Bad fit example (2)

3.2 Measurements

Datasets for three different overvoltages (3V, 4V and 6V) were taken and the gain extracted. The signals were sampled at the highest amplitudes to achieve maximum gain and a correction for the channel dependent breakdown voltage was applied. As demonstrated in figure 16, a linear fit delivered the slopes:

For $2\,\mathrm{mm}^2$ SiPMs: $(\frac{\Delta Gain}{\Delta OV})_{2mm^2} \approx (1.85 \pm 0.07)/V$
For $4\,\mathrm{mm}^2$ SiPMs: $(\frac{\Delta Gain}{\Delta OV})_{4mm^2} \approx (1.34 \pm 0.13)/V$

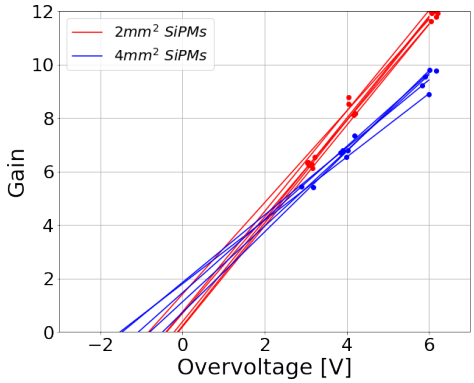

Figure 16: Gain measurement at different overvoltages

Ideally, one would expect all slopes to pass the point of origin. Why this is not the case for the data shown here, could be due to the systematic uncertainties in the experiments caused primarily by the limited gain resolution. Furthermore, the deviation between the $2\,\mathrm{mm}^2$ and $4\,\mathrm{mm}^2$ SiPMs was not expected. However, a possible explanation for that is the signal integration time. Both SiPM types are designed to have the same gain, but the SiPM area affects the effective SiPM capacitance, which leads to different pulse shapes. As the signal integration time does not cover the whole pulse, the larger SiPM area leads to a lower gain. (figure 17)

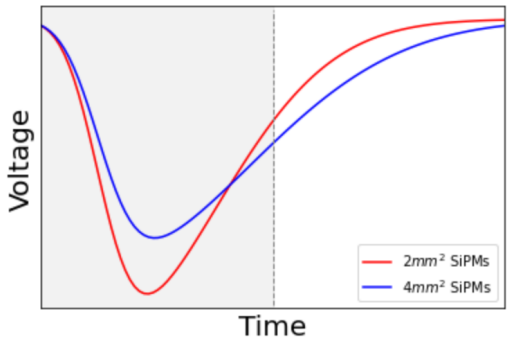

Figure 17: Different pulse shapes for the SiPMs

The next step was to take datasets at temperatures down to -40 $°C$ and investigate the temperature dependence of the gain. A linear fit delivers a slope of $(\frac{\Delta Gain}{\Delta T}) \approx -0.05/°C$ (figure 18). With this value and the previously calculated $(\frac{\Delta Gain}{\Delta OV})$ -value, the $(\frac{\Delta OV}{\Delta T})$-gradient could be calculated and the following values were received:

$(\frac{\Delta OV}{\Delta T}) = (\frac{\Delta Gain}{\Delta T})/(\frac{\Delta Gain}{\Delta OV})$

For $2\,\mathrm{mm}^2$ SiPMs: $(\frac{\Delta OV}{\Delta T})_{2mm^2} \approx (33 \pm 2) mV/K$

For $4\,\mathrm{mm}^2$ SiPMs: $(\frac{\Delta OV}{\Delta T})_{4mm^2} \approx (31 \pm 1) mV/K$

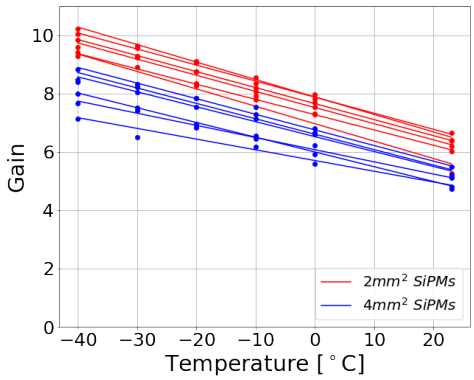

Figure 18: Gain measurement at different temperatures

In comparison to each other, the two gradients agree within their uncertainties. When comparing to the SiPM data sheet that states a slope of $(\Delta OV/\Delta T) \approx 34 mV/K$ [5], the measured gradient is within the uncertainties for the $2\,\mathrm{mm}^2$ SiPMs and deviates by 3σ for the $4\,\mathrm{mm}^2$ SiPMs. Further investigations should be applied due to the slight deviation. A possible start would be to check if the gains of the current conveyor and preamplifier stay constant with temperature.

4 Temperature studies of irradiated SiPMs

Additionally to the studies of the non-irradiated SiPMs, the temperature impact on the noise-level for the irradiated SiPMs was investigated. Therefore, a tileboard was used that consists of 2 SiPMs (one 2 mm^2 and one 4 mm^2 SiPM), which were irradiated to $2 \cdot 10^{12} n/cm^2$ which is equivalent to $5 \cdot 10^{13} n/cm^2$ at -30°C (maximum end-of-lifetime dose expected for SiPMs at the end-cap calorimeter). [3]

Radiated SiPMs have a very high noise level of 18 to 20 ADC RMS at room temperature, so that a signal is not clearly visible. For comparison: The RMS for non-irradiated SiPMs is around 1.5 ADC. However, lowering the temperature reduces the noise level. To validate and further investigate this behaviour, the goal was to measure the noise level at different temperature while maintaining a constant overvoltage to ensure a constant signal size. As the overvoltage is temperature dependent itself, additional adaptions had to be made to ensure a constant overvoltage within the whole temperature range. In more detail, lowering the temperature reduces the SiPM's breakdown voltage, which without a bias-voltage adjustment leads to an increasing overvoltage. This can be compensated by changing an HGCROC parameter (Input-DAC), with which the bias-voltage and thereby the OV can be decreased again. To calculate the needed Input-DAC-adaption, the following equation was used:

$$OV(T_1) = OV(T_0) - \Delta T \cdot (\tfrac{\Delta OV}{\Delta T}) + \Delta InputDAC \cdot (\tfrac{\Delta OV}{\Delta InputDAC})$$

With this equation, one can calculate the supplied overvoltage at room temperature ($OV(T_1)$) needed to keep the overvoltage at -30°C at 2 V ($OV(T_0)$), using the two known gradients ($\frac{\Delta OV}{\Delta T}$ from previous chapter and the OV dependence of the InputDAC) as well as the temperature difference ΔT and the applied change in Input-DAC $\Delta InputDAC$. However, changing the Input-DAC also changes the pedestal level, which needed to be adjusted again using a different HGCROC parameter. Concerning all these adaptions, a constant overvoltage was achieved.

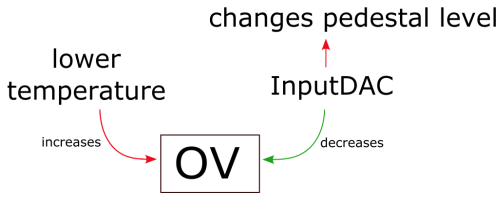

Figure 19: Overview OV-adjustments

The next step was to validate this method by measuring the gain at different temperatures while adjusting the InputDAC accordingly. If the adjustments are correct, the overvoltage and therefore the gain should be the same for all temperatures. As seen in figure 20, the percentage gain difference for temperature measurements at 0°C and

13°C is mostly within 10 percent, but a strong channel dependence is visible. A possible explanation for this is a temperature gradient on the readout chip, but further investigations are needed to validate this assumption.

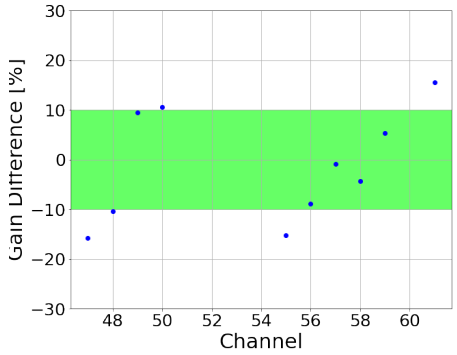

Figure 20: Gain difference for temperature measurements at $0°C$ and $13°C$

The last step was the measurement of the RMS of the irradiated SiPMs at temperatures down to -30°C while maintaining a constant OV of 2V using the procedure described above. As expected, one can see in figure 21 that the noise decreases with lower temperature. However, when applying a model that was conducted from experimental results by other groups within the HGCAL-group (using individual irradiated SiPMs and different readout electronics) on our data, the fit did not converge. A possible explanation is that many SiPM parameters are affected by temperature additionally to the breakdown voltage, e.g. dark count rates/leakage current. One other explanation is that because of the temperature gradient mentioned earlier, the two channels are again at a different overvoltage than expected. Additional investigation and adaption will be needed to ensure a constant OV over all temperatures.

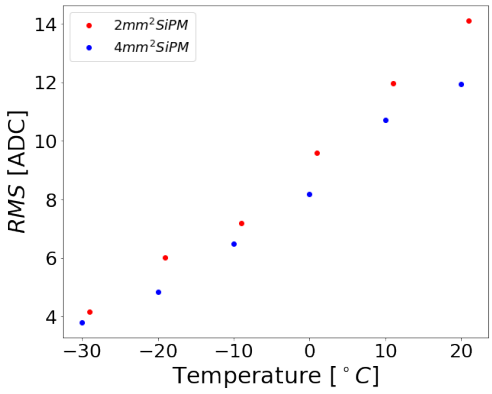

Figure 21: Temperature dependence of the noise

5 Summary and Outlook

It was possible to verify that the tileboard works stable at temperatures down to -40°C. For further measurements on the SiPMs, a method to correct for the Differential Non-Linearity was applied successfully for the first time. Out of the measured data, the $(\frac{\Delta OV}{\Delta T})$-coefficient was calculated. The slight deviation from the value provided by the datasheet could be due to a temperature dependence of the gains of the current conveyor and preamplifier. At this point, further investigations are ongoing. The coefficient was then used to measure the noise levels for irradiated SiPMs at low temperatures using a constant OV. As described above, it is much likely that many SiPM parameters are affected by temperature additional to the breakdown voltage, so that further investigations are needed considering all the factors that can influence the OV.

References

[1] URL: `https://home.cern/science/experiments/cms`. (accessed: 07.09.2021).

[2] Mathias Reinecke. *The CMS High Granularity Calorimeter Scintillator/SiPM Tileboards*. TIPP Conference. 2021.

[3] Malinda de Silva. *Beam Tests of the First CMS HGCAL Tileboard Prototypes*. DPG Talk. 2020.

[4] URL: `https://electronics360.globalspec.com/article/10397/pin-vs-apd-different-sensitivity-different-applications`. (accessed: 07.09.2021).

[5] Hamamatsu. *specification sheet, MPPC S14160-976x series*. Apr. 2020.